POINTWISE ANTENNAS DESIGN IN HYPERTHERMIA THERAPY

R. MATTOSO AND A.A. NOVOTNY*

Abstract. This work deals with pointwise antennas design in hyperthermia treatment. Hyperthermia is a non-invasive therapy usually combined with chemotherapy and/or radiotherapy, which consists in heating the diseased tissue in an attempt to kill the cancerous cells. In particular, we want to find the optimal values of current densities passing through each antenna to selectively heat a specified target. The forward problem is governed by the steady-state heat equation in living tissues which is coupled with the Helmholtz problem modeling the electromagnetism phenomenon. An objective functional measuring the difference between the target temperature and the solution to the model problem is minimized with respect to the current densities by using the topological derivative method. The resulting sensitivities are used to devise first and second order antenna design algorithms as well as a third one that combines both the previous algorithms. Numerical experiments are presented showing different features of the proposed methodology, including its capability in selectively heating the target up to the desired temperature. Finally, a selected result is used in a full transient analysis, where the hot spots are keeping over the diseased tissues during the whole heating process.

1. Introduction

Disordered cell growth, usually called cancer, is a common disease that affects the entire world population and can develop in any part of the human body. According to a World Health Organization's report [29], there were 18.1 million new diagnoses and 9.6 million cancer deaths worldwide in 2018. This same report points out that breast cancer ranks second in newly diagnosed cases and is also the fifth more fatal kind of cancer. The observed increase in the number of cancer cases is related to many factors, including population growth and its aging, economic development, and dietary patterns [4]. In some situations, there is a possibility of preventing the onset of cancer. For example, lung cancer is the leader in newly diagnosed cases, which in most of the time is a consequence of cigarette addiction [29]. There is also an expectation that new research will be able to assist in the prevention and cure of cancer with the aid of therapeutic vaccines [23, 24]. However, there are still no conclusive results on the effectiveness of these vaccines as shown in [26] work. Thus, what remains for now is to develop more efficient and less invasive treatments. The most common treatments for cancer are surgery, chemotherapy, radiotherapy, bone marrow transplantation, and also hyperthermia that can be used alone or combined with other treatments [31]. Chemotherapy and radiotherapy, when combined with hyperthermia therapy, become more effective allowing to be administered in lower doses. Hyperthermia consists in heating the tumor to a certain temperature, usually between 40°C and 46°C [8, 20]. The heating of cells – both healthy and diseased – may cause their death, so that it is important to selectively heat the tumor for preventing the death of healthy cells [12]. This is in fact the main challenge in hyperthermia therapy, which has motivated many recent studies [10].

Key words and phrases. Hyperthermia therapy, pointwise antenna design, heat equation, Helmholtz equation, topological derivative method.

*Corresponding author.

The paper [1] deals with topology design of electromagnetic distributed antennas. A gradient type method has been proposed, which successfully heat a single target per once. In contrast with [1], in this paper we propose a novel approach for pointwise antennas design in hyperthermia treatment that selectively heat several targets simultaneously up to the desired temperature. The model problem is governed by the steady-state heat equation in living tissues which is coupled with the Helmholtz problem modelling the electromagnetism phenomenon. The basic idea consists in finding the optimal values of current densities passing through each antenna. In particular, an objective functional measuring the difference between the target temperature and the solution to the model problem is minimized with respect to the current densities. The sensitivity analysis is explicitly written in the form of a fourth order expansion with respect to the current densities, which can be seen as the main theoretical contribution of the paper. The resulting sensitivities are used to devise first and second order antenna design algorithms as well as a third one that combines both the previous algorithms. Numerical experiments are presented showing different features of the proposed approach. Finally, a selected result is used in a full transient analysis, where the hot spots are keeping over the diseased tissues during the whole heating process.

This paper is organized as follows. The model problem we are dealing with is presented in Section 2. In Section 3 the Adjoint Sensitivity Method is used to obtain the associated derivatives. Based on the resulting sensitivities, three antenna design algorithms are proposed in Section 4. Some numerical experiments are presented in Section 5, showing different features of the first, second and combined algorithms. Finally, the paper ends with some concluding remarks in Section 6.

2. Problem Formulation

Let us consider an open and bounded domain $\Omega \subset \mathbb{R}^2$ with Lipschitz boundary $\partial\Omega$. Let $\mathcal{B} \subset \Omega$ and $\mathcal{D} \subset \mathcal{B}$ represent the tissue and the target to be burned, respectively. The pointwise antennas are represented by Dirac masses and belong to the set of admissible solutions $C_\delta(\Omega)$, which will be defined later on. See sketch in Figure 1.

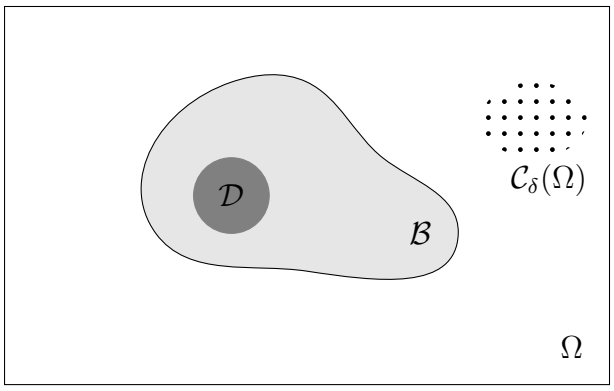

Figure 1. Problem setting.

Our goal is to find the optimal values of current densities passing through each antenna to selectively heat the target $\mathcal{D}$. Therefore, the following objective functional is introduced:

$$\mathcal{J}(\theta) = \beta_1 \int_{\mathcal{D}} (\theta - \theta^*)^2 + \beta_2 \int_{\mathcal{B}\setminus\mathcal{D}} (\theta - \theta_b)^2, \tag{2.1}$$

where $\theta^* : \mathbb{R}^2 \mapsto \mathbb{R}$ and $\theta_b : \mathbb{R}^2 \mapsto \mathbb{R}$ are the target and the blood temperatures, respectively. The weights $\beta_1 = \frac{\beta}{|\mathcal{D}|}$ and $\beta_2 = \frac{1-\beta}{|\mathcal{B}\backslash\mathcal{D}|}$, with $\beta \in (0,1)$. Finally, $\theta : \Omega \mapsto \mathbb{R}$ is the body temperature, solution to the following steady-state heat problem for live tissues [25, 30]:

$$\theta \in \mathcal{V} : \int_\Omega [K\nabla\theta \cdot \nabla\eta + c_b w(\theta - \theta_b)\eta] = \frac{1}{2}\int_\Omega \sigma|u|^2\eta, \quad \forall \eta \in \mathcal{V}_0, \tag{2.2}$$

where $K : \mathbb{R}^2 \mapsto \mathbb{R}$ is the thermal conductivity of the tissue [$\mathrm{Wm}^{-1\circ}\mathrm{C}^{-1}$], $c_b : \mathbb{R}^2 \mapsto \mathbb{R}$ is the specific heat of the blood, $w : \mathbb{R}^2 \mapsto \mathbb{R}$ is the blood perfusion rate [$\mathrm{kgm}^{-3}\ \mathrm{s}^{-1}$] and $\sigma : \mathbb{R}^2 \mapsto \mathbb{R}$ is the electrical conductivity of the medium [Sm^{-1}]. The set $\mathcal{V}$ and the space $\mathcal{V}_0$ are defined as

$$\mathcal{V} := \{\phi \in H^1(\Omega) : \phi_{|\partial\Omega} = \theta_\Gamma\} \quad \text{and} \quad \mathcal{V}_0 := H_0^1(\Omega), \tag{2.3}$$

where θ_Γ is a prescribed temperature on the boundary $\partial\Omega$. In addition, $u : \Omega \mapsto \mathbb{C}$ is solution to the Helmholtz problem [13], namely

$$u \in \mathcal{W}^{1,p}(\Omega) : \int_\Omega \left(\nabla u \cdot \nabla\bar{\eta} - k^2 u\bar{\eta}\right) + \mathbf{i}\int_{\partial\Omega} ku\bar{\eta} = \int_\Omega f\bar{\eta}, \quad \forall \bar{\eta} \in \mathcal{W}^{1,q}(\Omega) \tag{2.4}$$

where $\bar{(\cdot)}$ is the complex conjugate of $(\cdot)$ and $\mathcal{W}^{1,p}(\Omega)$ is a complex valued Sobolev space [3], such that

$$\frac{1}{p} + \frac{1}{q} = 1, \quad \text{with} \quad 1 \le p < 2. \tag{2.5}$$

The symbol $\mathbf{i}$ is used to denote the complex unit, such that $\mathbf{i} = \sqrt{-1}$. The wave number $k : \mathbb{R}^2 \mapsto \mathbb{R}$ is given by

$$k = \omega\sqrt{\varepsilon\mu}, \tag{2.6}$$

where ω is the angular frequency [Hz], $\varepsilon = \varepsilon_r\varepsilon_0$ is the electrical permittivity [Fm^{-1}], $\mu = \mu_r\mu_0$ is the magnetic permeability [Hm^{-1}]. The quantities ε_r and μ_r are the relative electrical permittivity and magnetic permeability, respectively, whereas $\varepsilon_0 = 8.854\times10^{-12}$ Fm^{-1} is the electrical permittivity and $\mu_0 = 4\pi\times10^{-7}$ Hm^{-1} is the magnetic permeability, both associated with the free space. Finally, $f \in C_\delta(\Omega)$ is the source term representing the pointwise antennas, with

$$C_\delta(\Omega) = \left\{ f \in \mathcal{M}(\Omega) : f(x) = \sum_{i=1}^{N} \alpha_i\delta(x - x_i) \right\}, \tag{2.7}$$

in which $\mathcal{M}(\Omega)$ denotes the dual space of continuous functions in Ω with compact support on $\partial\Omega$ and $\delta(x-x_i)$ are used to denote Dirac masses with poles at $x_i \in \Omega\backslash\overline{\mathcal{B}}$, $i = 1, \cdots, N$, with N denoting the number of antennas. The quantity $\alpha_i \in \mathbb{R}$ is given by

$$\alpha_i = \omega\mu_0 J_e(x_i), \tag{2.8}$$

where $J_e(x_i)$ is the current density [Am^{-2}] passing through the i-th antenna. Since the unknown α_i is proportional to the current density $J_e(x_i)$, for the sake of presentation, from now on α_i is also called current density.

From the above elements, the constrained optimization problem we are dealing with can be stated as following:

$$\begin{cases} \underset{f\in C_\delta(\Omega)}{\text{minimize}}\ \mathcal{J}(\theta), \\ \text{subject to (2.2) and (2.4).} \end{cases} \tag{2.9}$$

In order to simplify further analysis, we introduce two adjoint problems which are coupled in a reverse sense. The adjoint heat equation is written as:

$$\varphi \in \mathcal{V}_0 : \int_\Omega K\nabla\varphi\cdot\nabla\eta + \int_\Omega c\omega\varphi\eta = 2\beta_1\int_{\mathcal{D}}(\theta^*-\theta)\eta + 2\beta_2\int_{\mathcal{B}\setminus\mathcal{D}}(\theta_b-\theta)\eta, \quad \forall\eta\in\mathcal{V}_0, \tag{2.10}$$

whereas the adjoint Helmholtz problem is stated as:

$$v \in \mathcal{W}^{1,q}(\Omega) : \int_\Omega \big(\nabla v\cdot\nabla\bar{\eta} - k^2 v\bar{\eta}\big) - \mathbf{i}\int_{\partial\Omega} kv\bar{\eta} = -\int_\Omega \sigma\varphi u\bar{\eta}, \quad \forall\eta\in\mathcal{W}^{1,p}(\Omega). \tag{2.11}$$

3. Adjoint Sensitivity Analysis

In this section the necessary optimality conditions for the optimization problem (2.9) are derived in the spirit of the topological derivative method [21, 22, 27]. The basic idea consists in introducing a perturbation on the right-hand side of problem (2.4) of the form

$$f_\delta(x) = f(x) + \sum_i \alpha_i\delta_i(x), \tag{3.1}$$

where $\delta_i(x) := \delta(x - x_i)$, so that $f_\delta \in C_\delta(\Omega)$, with the summation defined from $i = N + 1$ up to $M > N$. The perturbed counterpart of the objective functional (2.1) is given by:

$$\mathcal{J}(\theta_\delta) = \beta_1\int_{\mathcal{D}}(\theta_\delta-\theta^*)^2 + \beta_2\int_{\mathcal{B}\setminus\mathcal{D}}(\theta_\delta-\theta_b)^2, \tag{3.2}$$

where the function θ_δ is solution to the perturbed heat conduction equation

$$\theta_\delta \in \mathcal{V} : \int_\Omega K\nabla\theta_\delta\cdot\nabla\eta + \int_\Omega c_b w(\theta_\delta-\theta_b)\eta = \frac{1}{2}\int_\Omega \sigma|u_\delta|^2\eta, \quad \forall\eta\in\mathcal{V}_0 \tag{3.3}$$

and u_δ is solution to the perturbed Helmholtz problem

$$u_\delta \in \mathcal{W}^{1,p}(\Omega) : \int_\Omega \big(\nabla u_\delta\cdot\nabla\bar{\eta} - k^2 u_\delta\bar{\eta}\big) + \mathbf{i}\int_{\partial\Omega} ku_\delta\bar{\eta} = \int_\Omega f_\delta\bar{\eta}, \quad \forall\eta\in\mathcal{W}^{1,q}(\Omega). \tag{3.4}$$

Let us propose the following *ansätze* for the solutions to the perturbed Helmholtz and heat conduction problems, respectively

$$u_\delta = u + \sum_i \alpha_i u_i, \tag{3.5}$$

$$\theta_\delta = \theta + \sum_i \alpha_i\theta_i + \sum_{ij}\alpha_i\alpha_j\theta_{ij}, \tag{3.6}$$

where u_i are solutions to the set of canonical variational problems of the form

$$u_i \in \mathcal{W}^{1,p}(\Omega) : \int_\Omega \big(\nabla u_i\cdot\nabla\bar{\eta} - k^2 u_i\bar{\eta}\big) + \mathbf{i}\int_{\partial\Omega} ku_i\bar{\eta} = \int_\Omega \delta_i\bar{\eta}, \quad \forall\eta\in\mathcal{W}^{1,q}(\Omega) \tag{3.7}$$

whereas θ_i and θ_{ij} are respectively solutions to the following variational problems

$$\theta_i \in \mathcal{V}_0 : \int_\Omega K\nabla\theta_i\cdot\nabla\eta + \int_\Omega c_b w\theta_i\eta = \int_\Omega \sigma\mathrm{Re}\{u\bar{u}_i\}\eta, \quad \forall\eta\in\mathcal{V}_0, \tag{3.8}$$

$$\theta_{ij} \in \mathcal{V}_0 : \int_\Omega K\nabla\theta_{ij}\cdot\nabla\eta + \int_\Omega c_b w\theta_{ij}\eta = \frac{1}{2}\int_\Omega \sigma\mathrm{Re}\{u_i\bar{u}_j\}\eta, \quad \forall\eta\in\mathcal{V}_0. \tag{3.9}$$

After replacing the *ansatz* (3.6) into (3.2), we obtain

$$\begin{aligned}\mathcal{J}(\theta_\delta)-\mathcal{J}(\theta)=\beta_1\int_{\mathcal{D}}\Big[&2(\theta-\theta^*)\sum_i\alpha_i\theta_i+2(\theta-\theta^*)\sum_{ij}\alpha_i\alpha_j\theta_{ij}\\&+\sum_{ij}\alpha_i\alpha_j\theta_i\theta_j+2\sum_{ijk}\alpha_i\alpha_j\alpha_k\theta_{ij}\theta_k+\sum_{ijkl}\alpha_i\alpha_j\alpha_k\alpha_l\theta_{ij}\theta_{kl}\Big]\\&+\beta_2\int_{\mathcal{B}\setminus\mathcal{D}}\Big[2(\theta-\theta_b)\sum_i\alpha_i\theta_i+2(\theta-\theta_b)\sum_{ij}\alpha_i\alpha_j\theta_{ij}\\&+\sum_{ij}\alpha_i\alpha_j\theta_i\theta_j+2\sum_{ijk}\alpha_i\alpha_j\alpha_k\theta_{ij}\theta_k+\sum_{ijkl}\alpha_i\alpha_j\alpha_k\alpha_l\theta_{ij}\theta_{kl}\Big].\end{aligned}\tag{3.10}$$

which represents the exact sensitivity of the objective functional with respect to the introduction of a number $M-N$ additional pointwise antennas. In particular, we can recognize first, second, third and fourth orders derivatives associated with to the terms multiplied by α_i, $\alpha_i\alpha_j$, $\alpha_i\alpha_j\alpha_k$ and $\alpha_i\alpha_j\alpha_k\alpha_l$, respectively.

The sensitivity (3.10) can be used to devise reconstruction algorithms which find the optimal locations $x_i^\star$ for the antennas as well as their optimal currents $\alpha_i^\star$, similarly to proposed by [16]. However, we assume that the locations x_i are given and the optimal currents $\alpha_i^\star$ have to be found, which allows to drop the summations in (3.10) from $1,\cdots,N$. Even in this scenario, the use of the sensitivity formula (3.10) still requires further simplification. Actually, the computation of all terms in (3.10) becomes unfeasible due to the combinatorial nature of problems for θ_{ij} from (3.9). Therefore, our strategy is to truncate (3.10) up to the second order term. In particular, the following quantity is introduced:

$$\begin{aligned}\Psi(\alpha_1,\alpha_2,...,\alpha_N)=\beta_1\int_{\mathcal{D}}&\Big[2(\theta-\theta^*)\sum_i\alpha_i\theta_i+2(\theta-\theta^*)\sum_{ij}\alpha_i\alpha_j\theta_{ij}+\sum_{ij}\alpha_i\alpha_j\theta_i\theta_j\Big]\\&+\beta_2\int_{\mathcal{B}\setminus\mathcal{D}}\Big[2(\theta-\theta_b)\sum_i\alpha_i\theta_i+2(\theta-\theta_b)\sum_{ij}\alpha_i\alpha_j\theta_{ij}+\sum_{ij}\alpha_i\alpha_j\theta_i\theta_j\Big],\end{aligned}\tag{3.11}$$

where the summation is now defined from $i=1$ up to N, with N used to denote a given number of antennas. Equation (3.11) can be conveniently written in a compact form as

$$\Psi(\alpha)=\mathrm{d}\cdot\alpha+\mathrm{H}\alpha\cdot\alpha,\tag{3.12}$$

where $\alpha=(\alpha_1,\alpha_2,...,\alpha_N)^\top$, $\mathrm{d}=(d_1,d_2,...,d_N)^\top$ is the first order derivative with entries

$$d_i=2\beta_1\int_{\mathcal{D}}(\theta-\theta^*)\theta_i+2\beta_2\int_{\mathcal{B}\setminus\mathcal{D}}(\theta-\theta_b)\theta_i,\tag{3.13}$$

and H is the second order derivative whose entries are given by

$$H_{ij}=\beta_1\int_{\mathcal{D}}\big[2(\theta-\theta^*)\theta_{ij}+\theta_i\theta_j\big]+\beta_2\int_{\mathcal{B}\setminus\mathcal{D}}\big[2(\theta-\theta_b)\theta_{ij}+\theta_i\theta_j\big],\tag{3.14}$$

with θ solution to the heat problem (2.2), θ_i solutions to the variational problems (3.8) and θ_{ij} solutions to the variational problems (3.9).

4. Antenna Design Algorithms

In this section, we present first and second order methods as well as a third one that combines both the previous methods for solving the optimization problem (2.9) with help of (3.12).

4.1. **First Order Method.** From (3.12), we can define the following quantity

$$\Psi_1(\alpha) := \mathrm{d} \cdot \alpha. \tag{4.1}$$

In order to evaluate (4.1) the canonical problems (3.7) and (3.8) have to be solved for each point x_i, $i = 1, \cdots, N$. Instead, we evoke the adjoint sensitivity method which allows for simplifying such computations. Actually, by setting $\eta = \varphi$ in (3.8) and $\eta = \theta_i$ in (2.10), we obtain

$$\int_\Omega K\nabla\theta_i \cdot \nabla\varphi + \int_\Omega cw\theta_i\varphi = \int_\Omega \sigma\varphi \mathrm{Re}\{u\bar{u}_i\}, \tag{4.2}$$

$$\int_\Omega K\nabla\varphi \cdot \nabla\theta_i + \int_\Omega cw\varphi\theta_i = 2\beta_1 \int_{\mathcal{D}} (\theta^* - \theta)\theta_i + 2\beta_2 \int_{\mathcal{B}\setminus\mathcal{D}} (\theta_b - \theta)\theta_i. \tag{4.3}$$

From the symmetry of both bilinear forms, the following equality holds true:

$$\int_\Omega \sigma\varphi \mathrm{Re}\{u\bar{u}_i\} = 2\beta_1 \int_{\mathcal{D}} (\theta^* - \theta)\theta_i + 2\beta_2 \int_{\mathcal{B}\setminus\mathcal{D}} (\theta_b - \theta)\theta_i. \tag{4.4}$$

Therefore, equation (3.13) can be rewritten as

$$d_i = -\int_\Omega \sigma\varphi \mathrm{Re}\{u\bar{u}_i\}, \tag{4.5}$$

where φ is solution to the variational problem (2.10). Now, let us take $\eta = v$ in (3.7) and $\eta = u_i$ in (2.11), to obtain

$$\int_\Omega \left(\nabla u_i \cdot \nabla\bar{v} - k^2 u_i\bar{v}\right) + \mathbf{i}\int_{\partial\Omega} k u_i\bar{v} = \int_\Omega \delta_i\bar{v}, \tag{4.6}$$

$$\int_\Omega \left(\nabla v \cdot \nabla\bar{u}_i - k^2 v\bar{u}_i\right) - \mathbf{i}\int_{\partial\Omega} k v\bar{u}_i = -\int_\Omega \sigma\varphi u\bar{u}_i. \tag{4.7}$$

From a simple manipulation, equation (4.7) can be rewritten as

$$\int_\Omega \left(\nabla u_i \cdot \nabla\bar{v} - k^2 u_i\bar{v}\right) + \mathbf{i}\int_{\partial\Omega} k u_i\bar{v} = -\int_\Omega \sigma\varphi u\bar{u}_i. \tag{4.8}$$

After comparing (4.6) with (4.8), we obtain the following important equality

$$\int_\Omega \delta_i\bar{v} = -\int_\Omega \sigma\varphi u\bar{u}_i. \tag{4.9}$$

By taking the real part on both sides of (4.9), equation (4.5) can be rewritten as

$$d_i = \mathrm{Re}\{\bar{v}(x_i)\}, \tag{4.10}$$

where v is solution to the adjoint problem (2.11).

Now we have all elements to devise a gradient descent algorithm. The basic idea consists in use the first order gradient d as a descent direction, so that we set $\alpha = -\gamma\mathrm{d}$, with $\gamma > 0$. In particular, the weight γ is defined as

$$\gamma := \frac{\mathcal{J}(\theta)}{\|\mathrm{d}\|^2}. \tag{4.11}$$

Then, quantity α can be updated as follows

$$\alpha \leftarrow \alpha - \gamma\mathrm{d}. \tag{4.12}$$

The resulting first order method written in pseudo-code format is summarized through Algorithm 1, where the parameters ϵ_J and ϵ_γ are user-defined stop criteria.

Algorithm 1: First Order

Input: α
Parameter: $\epsilon_\gamma, \epsilon_J$
Output: $\alpha^\star$
begin
  Compute: u, θ and $\mathcal{J}(\theta)$
  $\gamma \leftarrow 1$
  $\delta_J \leftarrow \mathcal{J}(\theta)$
  $J_{old} \leftarrow \mathcal{J}(\theta)$
  while $\delta_J > \epsilon_J$ ***and*** $\gamma > \epsilon_\gamma$ **do**
    Compute: φ, v, d and γ
    $J_{new} \leftarrow J_{old} + 1$
    $\alpha_{old} \leftarrow \alpha$
    while $J_{new} > J_{old}$ ***and*** $\gamma > \epsilon_\gamma$ **do**
      $\alpha = \alpha_{old} - \gamma \mathrm{d}$
      Compute: u, θ and $\mathcal{J}(\theta)$
      $J_{new} \leftarrow \mathcal{J}(\theta)$
      $\gamma = \gamma/2$
    end while
    $\delta_J \leftarrow J_{old} - J_{new}$
    $J_{old} \leftarrow J_{new}$
  end while
  $\alpha^\star \leftarrow \alpha$
end

4.2. **Second Order Method.** From (3.12), we can define the following quantity

$$\Psi_2(\alpha) := \Psi(\alpha), \tag{4.13}$$

depending on the canonical problems (3.7) and (3.8) as well as (3.9), which have to be solved for each point x_i, $i = 1, \cdots, N$. Therefore, let us evoke again the adjoint sensitivity method in order to simplify such a computations. Note however that the product $\theta_i\theta_j$ in (3.11) cannot be absorbed by any adjoint state. Thus, let us focus our attention to θ_{ij} in (3.11). By setting $\eta = \varphi$ in (3.9) and $\eta = \theta_{ij}$ in (2.10) as test functions, we obtain

$$\int_\Omega K\nabla\theta_{ij}\cdot\nabla\varphi + \int_\Omega c_b w\theta_{ij}\varphi = \frac{1}{2}\int_\Omega \sigma\varphi \mathrm{Re}\{u_i\bar{u}_j\}, \tag{4.14}$$

$$\int_\Omega K\nabla\varphi\cdot\nabla\theta_{ij} + \int_\Omega c_b w\varphi\theta_{ij} = 2\beta_1\int_{\mathcal{D}}(\theta^* - \theta)\theta_{ij} + 2\beta_2\int_{\mathcal{B}\setminus\mathcal{D}}(\theta_b - \theta)\theta_{ij}. \tag{4.15}$$

From the symmetry of the above bilinear forms, the following equality holds true

$$\frac{1}{2}\int_\Omega \sigma\varphi \mathrm{Re}\{u_i\bar{u}_j\} = 2\beta_1\int_{\mathcal{D}}(\theta^* - \theta)\theta_{ij} + 2\beta_2\int_{\mathcal{B}\setminus\mathcal{D}}(\theta_b - \theta)\theta_{ij}, \tag{4.16}$$

allowing to rewrite the entries of the matrix H as

$$H_{ij} = \beta_1\int_{\mathcal{D}}\theta_i\theta_j + \beta_2\int_{\mathcal{B}\setminus\mathcal{D}}\theta_i\theta_j - \frac{1}{2}\int_\Omega \sigma\varphi\mathrm{Re}\{u_i\bar{u}_j\}, \tag{4.17}$$

where φ is solution to the adjoint heat equation (2.10).

In order to avoid unfeasible high current densities, we state the following constrained minimization problem

$$\begin{cases} \underset{\alpha\in\mathbb{R}^N}{\text{minimize}}\ \Psi_2(\alpha) \\ \text{subject to } \|\alpha\| \leq \mathrm{L}, \end{cases} \tag{4.18}$$

with $\mathrm{L} > 0$. Problem (4.18) can be rewritten as an unconstrained minimization problem of the form

$$\underset{\alpha\in\mathbb{R}^N}{\text{minimize}}\ \Psi_2^{\lambda}(\alpha) := \Psi_2(\alpha) + \lambda\|\alpha\|^2, \tag{4.19}$$

where $\lambda > 0$ is a user-defined penalty parameter, which replaces the inequality constraint in (4.18). After applying the first order optimality condition in (4.19), we obtain

$$\langle D_\alpha \Psi_2^{\lambda}(\alpha), \beta\rangle = 0. \qquad \forall \beta \in \mathbb{R}^N. \tag{4.20}$$

From the symmetry of the matrix H, the optimal values for the current densities are obtained as solution to the following linear system

$$2(\mathrm{H} + \lambda \mathrm{I})\alpha = -\mathrm{d}, \tag{4.21}$$

where I is the N-dimensional identity matrix. As an external step control, quantity α is updated as follows

$$\alpha \leftarrow \alpha + \gamma \mathrm{d}, \tag{4.22}$$

in which $0 < \gamma \leq 1$ is obtained with help of a line-search procedure. The resulting second order method written in pseudo-code format is summarized through Algorithm 2, where the parameters ϵ_J and ϵ_γ are user-defined stop criteria.

Algorithm 2: SECOND ORDER

```
Input: α
Parameter: ε_γ, ε_J
Output: α*
begin
    Compute: u, u_i, θ and J(θ)
    δ_J ← J(θ)
    J_old ← J(θ)
    while δ_J > ε_J and γ > ε_γ do
        α_old ← α
        Compute: φ, θ_i, d, H and α
        J_new ← J_old + 1
        γ ← 1
        while J_new > J_old and γ > ε_γ do
            α ← α_old + γα
            Compute: u, θ and J(θ)
            J_new ← J(θ)
            γ ← γ/2
        δ_J ← J_old − J_new
        J_old ← J_new
    α* ← α
```

4.3. **Combined Method.** After replacing the canonical solutions θ_i and u_i by their respective adjoint solutions, the computational cost associated with each iteration of the first order Algorithm 1 becomes very low in comparison with the second order Algorithm 2, which still requires the evaluation of θ_i and u_i. On the other hand, it is expected that

Algorithm 2 will converge faster to a better solution than Algorithm 1. Therefore, we propose a third heuristic which consists in using the solution found by Algorithm 1 as initial guess for Algorithm 2 with $\lambda = 0$, allowing to take advantage from both algorithms.

5. Numerical Experiments

In this section we present some numerical experiments. The objective of those experiments is to show that the proposed methods can selectively heat a specific target. In the first example of Section 5.1, the working frequency and number of antennas are specified and a comparison between the three algorithms of Section 4 is presented. In Sections 5.2 and 5.3, the targets are given by circular and L-shape breast tumors, respectively. A prostate tumor is considered in Section 5.4. Finally, Section 5.5 shows an example concerning three circular breast tumors of different sizes. The result obtained from the steady-state analysis is validated in a more realistic scenario by considering the full transient regime.

The domain Ω is given by a square of size $(0.0, 0.5) \times (0.0, 0.5)\text{m}^2$. The antennas are uniformly distributed in Ω around the body $\mathcal{B}$, as shown in Figure 2(a). Since standard Galerkin method is used to discretize the BVPs, the *Ihlenburg-Babuška* condition has to be fulfilled, which is given by $k^2 h < 1$, where k is the wave number and h is the relative element mesh size [9]. In particular, approximately 820×10^3 triangular elements are used to discretize the domain Ω, ensuring that the solutions to the Helmholtz problems become stable. The mesh pattern is sketched in Figure 2(b). We set the weight $\beta = 0.5$ in the objective functional (3.10) and define the stopping criteria as $\epsilon_J = \epsilon_\gamma = 10^{-4}$. All the algorithms were coded in [17].

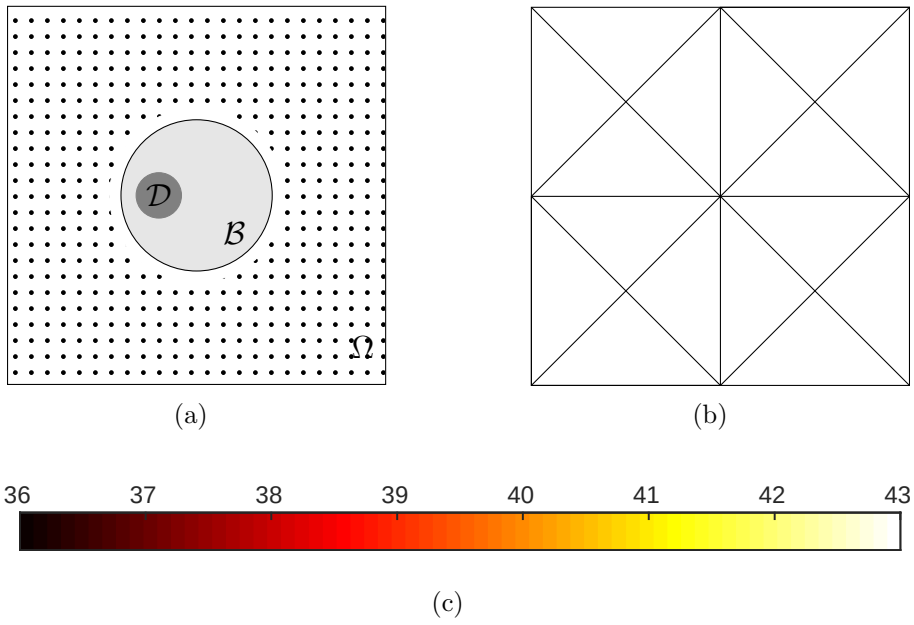

Figure 2. Experiments setting (a) finite elements mesh pattern (b) and temperature scale in Celsius (c).

The target and the normal body temperatures are defined as $\theta^* = 42°\text{C}$ and $\theta_b = 36°\text{C}$, respectively. The temperature $\theta_\Gamma = 25°\text{C}$ is prescribed on $\partial\Omega$. The specific heat of the blood is given by $c_b = 3850\ \text{Jkg}^{-1°}\text{C}^{-1}$ [5]. We also consider that $\mathcal{B}$ is surrounded by

deionized water [1, 30]. For the sake of comparison between the results, a temperature scale is fixed according to Figure 2(c).

5.1. **Example 1: Circular Target.** In this experiment, the body $\mathcal{B}$ is defined by a circle with center at $(0.25, 0.25)$ and 10.0cm of radius. It represents mammary tissue assumed to be composed of fat, for simplicity. The target $\mathcal{D}$ has 2.0cm of radius and center at $(0.28, 0.28)$. See sketch in Figure 3. The material properties used in this example are summarized in Table 1 [1, 11, 30]. Note that the region $\mathcal{D}$ has the same material properties as the background, so that it does not present as diseased tissue. Actually, $\mathcal{D}$ is just a target to be heated selectively, which makes the problem much more difficult, since normally the contrasting properties of the cancer induce selective heating of the target $\mathcal{D}$. We take advantage of this feature in the next experiments.

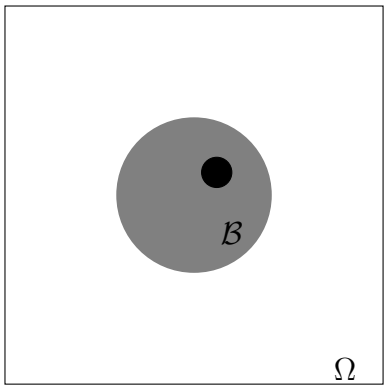

FIGURE 3. Example 1. Sketch of the healthy body on gray and of the target on black.

TABLE 1. Example 1. Material properties of the deionized water and mammary tissue.

	K [Wm°C^{-1}]	w [kgm^{-3}s]	ε_r [Fm^{-1}]	σ [Sm^{-1}]
Water	0.598	0.0	76.5	10^{-4}
Fat	0.20	1.1	20.0	0.12

5.1.1. *Working Frequency.* The frequency number is of significant importance for this work because it is directly related to the wave number k and – by consequence – to the solution of Helmholtz equation (2.4), so that the temperature pattern strongly depends on the frequency number through the heat problem (2.2). Therefore, three values in the frequency range currently found in the literature [1, 14, 30, 31] are considered, namely $\omega = 100, 200, 300$MHz. Note that in this range of frequency, the heating process is driven mainly by Ohmic effects. Since the electrical properties of biological tissues change according to the frequency number, we present in Table 2 [11] the three working frequencies to be considered together with the associated electrical permittivity and conductibility.

The number of antennas is fixed as $N = 36$. In order to chose the best working frequency, only the first order method is used to solve the optimization problem (2.9). The resulting temperature distributions are presented in Figure 4 for $\omega = 100$MHz (Figure 4(a), after 48 iterations and 1h 57min 19s, with $\mathcal{J}(\theta) = 4.9751$), $\omega = 200$MHz (Figure

TABLE 2. Example 1. Electrical biological properties considering frequency number.

ω [MHz]	ε_r [Fm^{-1}]	σ [Sm^{-1}]
100	20.5	0.11
200	20.2	0.12
300	20.0	0.12

4(b), after 25 iterations and 47min 59s, with $\mathcal{J}(\theta) = 3.0303$) and $\omega = 300$MHz (Figure 4(c), after 38 iterations and 1h 29min 37s, with $\mathcal{J}(\theta) = 1.6652$). As expected, the best result is obtained with the higher frequency, namely $\omega = 300$MHz, where the hot-spot is clearly over the target.

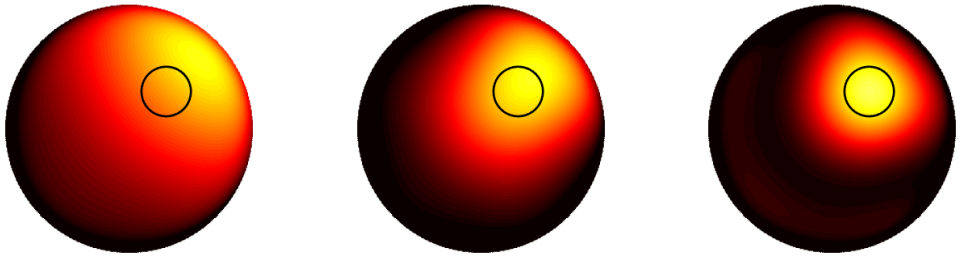

(a) (b) (c)

FIGURE 4. Example 1. Temperature distribution using 36 antennas. The target follows highlighted in solid black line. Obtained results for $\omega = 100$MHz (a), $\omega = 200$MHz (b) and $\omega = 300$MHz (c). See Figure 2(c).

5.1.2. *Number of Antennas.* It is expected that the number of antennas would have influence on the temperature distribution. Therefore, we fix the frequency as $\omega = 300$MHz and consider two different numbers of antennas, namely $N = 36$ and $N = 168$. Again, only the first order method is used to solve the optimization problem (2.9).

The resulting temperature distributions are presented in Figure 5, together with the final current densities. The centers of the circles represent the positions of the antennas and their radii are proportional to the obtained current densities $\alpha^\star$. Finally, positive sign means that the current flows out the page, otherwise the current flows into the page. In particular, Figure 5 shows the obtained results for $N = 36$ (Figure 5(a), after 38 iterations and 1h 29min 37s, with $\mathcal{J}(\theta) = 1.6652$) and $N = 168$ (Figure 5(b), after 39 iterations and 1h 35min 55s, with $\mathcal{J}(\theta) = 1.6439$). The obtained result for $N = 168$ is a bit better than the one for $N = 36$. For a higher number of antennas, the results were not significantly better than that obtained for $N = 168$.

5.1.3. *Methods Comparison.* In this section we compare the performance of the three devised algorithms of Section 4. The working frequency and number of antennas are fixed as $\omega = 300$MHz and $N = 168$, respectively. We start by comparing Algorithms 1 and 2 without regularization, that is we set $\lambda = 0.0$. In both cases the initial guess is given by an uniform current density $\alpha_i = 3 \times 10^2$, for $i = 1, \cdots, N$. For a smaller current density, the

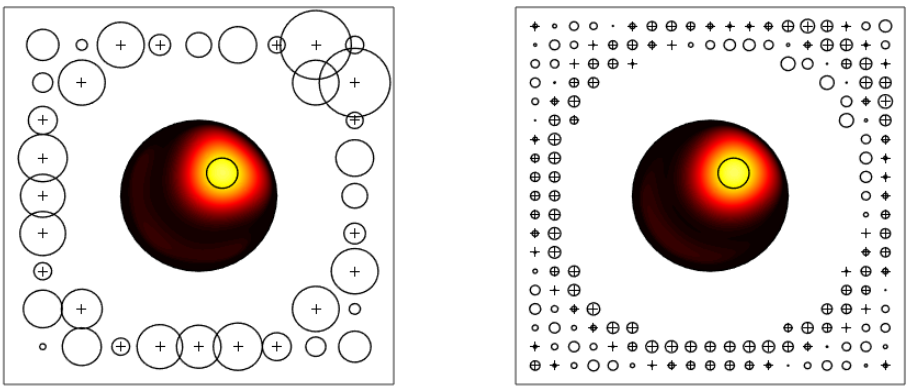

(a) (b)

FIGURE 5. Example 1. Temperature distribution for $\omega = 300$MHz. The target follows highlighted in solid black line. The centers of the circles represent the positions of the antennas and their radii are proportional to the obtained current densities $\alpha^\star$. Finally, positive sign means that the current flows out the page, otherwise the current flows into the page. Obtained results for $N = 36$ antennas (a) and $N = 168$ antennas (b). See also Figure 2(c).

second order method requires regularization. Figure 6 shows the obtained results for the first order method (Figure 6(a), after 50 iterations and 54min 21s, with $\mathcal{J}(\theta) = 1.6956$) and for the second order method (Figure 6(b), after 11 iterations and 2h 26min 26s, with $\mathcal{J}(\theta) = 1.6182$). The convergence histories of both algorithms are presented in Figure 7. Note that the second order method converges faster to a smaller value of the objective functional. However, it requires more than two times of CPU consuming with respect to the first order method.

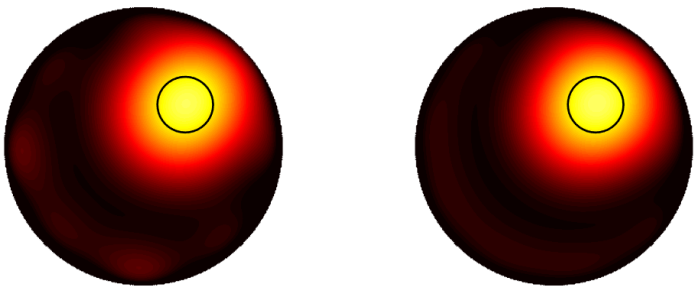

(a) (b)

FIGURE 6. Example 1. Temperature distribution for $\omega = 300$MHz and $N = 168$. The target follows highlighted in solid black line. Obtained results for the first order method (a) and for the second order method with $\lambda = 0.0$ (b). See also Figure 2(c).

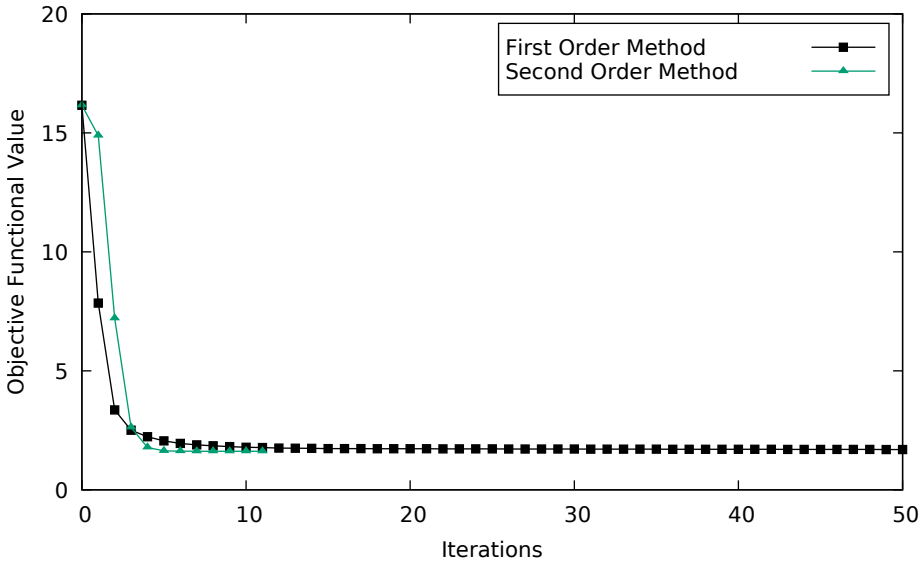

FIGURE 7. Example 1. Comparison between the objective functional values obtained during the iterative process.

Now, we set an uniform current density $\alpha_i = 1$, for $i = 1, \cdots, N$ as initial guess. In this case, the second order method requires regularization, so that we set $\lambda = 3 \times 10^{-5}$, which is the – empirically found – smallest value for the regularizing parameter. Figure 8 shows the obtained results for the first order method (Figure 8(a), after 39 iterations and 1h 35min 55s, with $\mathcal{J}(\theta) = 1.6439$) and for the second order method (Figure 8(b), after 58 iterations and 1d 8h 14min 10s, with $\mathcal{J}(\theta) = 1.6443$). Both results are quite similar in terms of temperature distribution and objective functional values. However, the second order method is much more time consuming than the first order method (more than 20 times).

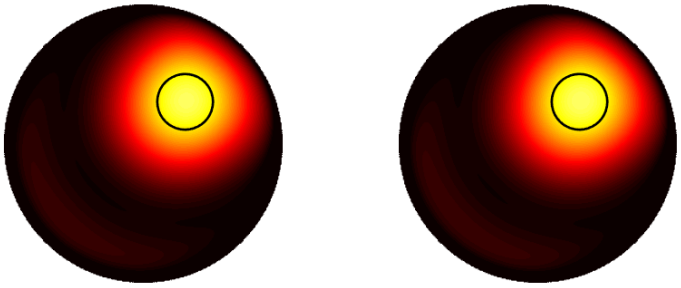

(a) (b)

FIGURE 8. Example 1. Temperature distribution for $\omega = 300$MHz and $N = 168$. The target follows highlighted in solid black line. Obtained results for the first order method (a) and for the second order method with $\lambda = 3 \times 10^{-5}$ (b). See also Figure 2(c).

Finally, in order to compare the performance of the combined method from Section 4.3 with Algorithms 1 and 2, we set the last current density obtained from the first order method as initial guess to the second order method, but with $\lambda = 0.0$. Figure 9 shows the

initial temperature distribution and final result for the combined method obtained after 40 iterations and 2h 34min 40s, with $\mathcal{J}(\theta) = 1.6438$. The combined algorithm converges to a little bit smaller value of the objective functional, with about 60% more time consuming than the first order method.

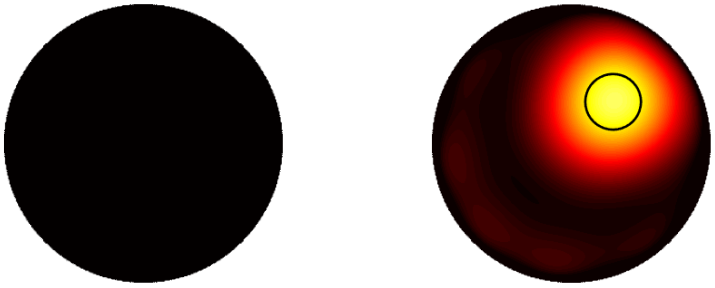

(a) (b)

FIGURE 9. Example 1. Temperature distribution for $\omega = 300$MHz and $N = 168$. The target follows highlighted in solid black line. Initial temperature distribution (a) and obtained result for the combined method (b). See also Figure 2(c).

Table 3 presents the minimum and maximum current densities values $J_e(x_i) = \alpha_i/(\omega\mu_0)$ obtained for each method by taking into account the last set of experiments.

TABLE 3. Example 1. Extremes current densities values $J_e(x_i) = \alpha_i/(\omega\mu_0)$ [Am^{-2}].

Method	Minimum	Maximum
First Order	-0.0773	0.0766
Second Order	-0.0767	0.0769
Combined	-16.2819	13.8939

Through this example it is shown that the three methods perform well in selectively heating a given target. However, the second order method either strongly depends on the initial guess or it is too time consuming after regularization. Therefore, in the next set of examples, only the first order algorithm and the combined method are used in order to perform further comparisons.

5.2. **Example 2: Circular Breast Tumor.** In this section, the target is finally characterized as a tumor, in the case a breast tumor, so that the same geometries for the healthy tissue $\mathcal{B}$ and target $\mathcal{D}$ as before are considered, but with $\mathcal{D}$ representing a diseased tissue. The material properties of the breast tumor $\mathcal{D}$ are summarized in Table 4 [1, 11, 30], whereas the remainder part are characterized according to Table 1. The working frequency and number of antennas are fixed as $\omega = 300$MHz and $N = 168$, respectively.

Figure 10 shows the initial temperature distribution, the obtained results for the first order method (Figure 10(b), after 35 iterations and 1h 28min 55s, with $\mathcal{J}(\theta) = 0.6135$) and for the combined method (Figure 10(c), after 42 iterations and 5h 42min 59s, with

TABLE 4. Example 2. Material properties of the breast tumor for $\omega = 300$MHz.

K [Wm°C^{-1}]	w [kgm^{-3}]	ε_r [Fm^{-1}]	σ [Sm^{-1}]
0.56	1.8	58.2	0.82

$\mathcal{J}(\theta) = 0.6125$). As expected, the hot spots are more concentrated over the target than in the previous example. This phenomenon occurs because the tumor is more vascularized, which induces a temperature increasing over it when exposed to the electromagnetic field. The model problem takes it into account mainly through the parameter σ, whose value is higher in the tumor than in the healthy tissue. See Figures 9(b) and 10(c) for homogeneous and heterogeneous media, respectively, where the heat is more concentrated within the tumor than in the target. Finally, Table 5 presents the minimum and maximum current densities values $J_e(x_i) = \alpha_i/(\omega\mu_0)$ obtained for both methods. In general, the first order method performs as good as the combined one, but with low computational cost (about 4 times faster).

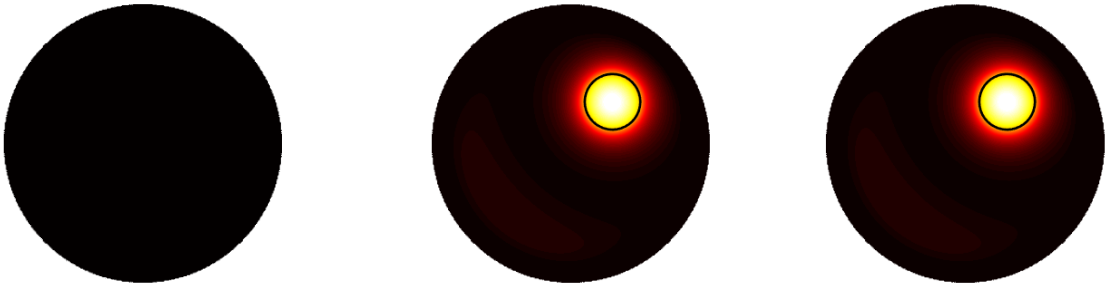

(a) (b) (c)

FIGURE 10. Example 2. Temperature distribution for $\omega = 300$MHz and $N = 168$. The tumor follows highlighted in solid black line. Initial temperature distribution (a) and obtained results for the first order method (b) as well as for the combined method (c). See also Figure 2(c).

TABLE 5. Example 2. Extremes current densities values $J_e(x_i) = \alpha_i/(\omega\mu_0)$ [Am^{-2}].

Method	Minimum	Maximum
First Order	-0.0329	0.0387
Combined	-0.0328	0.0385

5.3. **Example 3: L-Shaped Breast Tumor.** It is well known that the tumor may assume different shapes [18]. Therefore, let us consider the same example as before according to Tables 1 and 4, but with the target $\mathcal{D}$ representing a L-Shaped tumor with horizontal and vertical brackets of sizes 5.0cm $\times$ 1.0cm and 1.0cm $\times$ 4.0cm, respectively. See sketch in Figure 11. Again, the working frequency and number of antennas are set as $\omega = 300$MHz and $N = 168$, respectively.

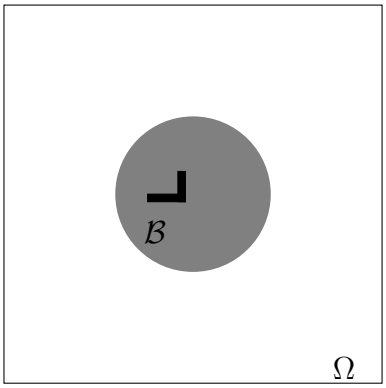

FIGURE 11. Example 3. Sketch of the healthy body on gray and of the L-Shaped tumor on black.

In Figure 12 it is shown the obtained results for the first order method (Figure 12(a), after 60 iterations and 2h 1min 7s, with $\mathcal{J}(\theta) = 0.8708$) and for the combined method (Figure 12(b), after 64 iterations and 4h 38min 30s, with $\mathcal{J}(\theta) = 0.8224$). In terms of objective functional value, the combined method performs better than the first order method, but with higher computational cost (more than 2 times). Therefore, in the next set of examples, only the combined method is used. Finally, Table 6 presents the minimum and maximum current densities values $J_e(x_i) = \alpha_i/(\omega\mu_0)$ obtained for both methods.

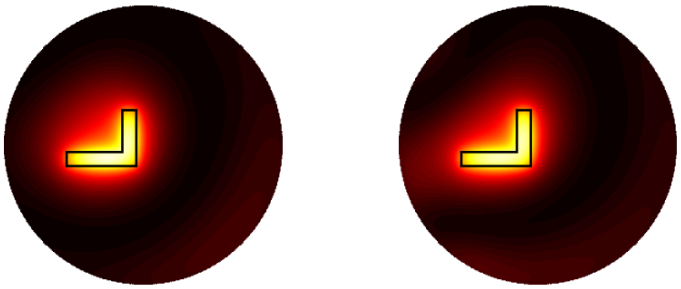

(a) (b)

FIGURE 12. Example 3. Temperature distribution for $\omega = 300$MHz and $N = 168$. The target follows highlighted in solid black line. Obtained results for the first order method (a) and for the combined method (b). See Figure 2(c).

TABLE 6. Example 3. Extremes current densities values $J_e(x_i) = \alpha_i/(\omega\mu_0)$ [Am^{-2}].

Method	Minimum	Maximum
First Order	-0.0500	0.0577
Combined	-0.1891	0.3393

5.4. **Example 4: Prostate Tumor.** In this section we consider a prostate tumor. Region $\mathcal{B}$ represents a man's abdominal cross section, which is assumed to be composed by bones, bladder, muscle and fat. The tumor has 2.0cm of radius and center at $(0.25, 0.21)$ within the prostate region. See sketch in Figure 13. The bladder is treated as a muscle, because it is assumed to be empty. The material properties for bladder, muscle and bones are summarized in Table 7 [6, 28], whereas the remainder part are characterized according to Tables 1 and 4 from the former examples. The working frequency and number of antennas are fixed as $\omega = 300$MHz and $N = 168$, respectively.

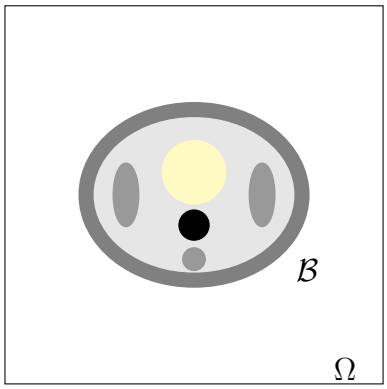

FIGURE 13. Example 4. Sketch of a man's abdominal cross section. Fat, bones and muscles are highlighted in dark gray, gray and light gray, respectively, whereas the bladder appears in yellow and the prostate tumor in black.

TABLE 7. Example 4. Material properties of the bladder, muscle and bones for $\omega = 300$MHz.

Tissue	K [Wm°C^{-1}]	w [kgm^{-3}]	ε_r [Fm^{-1}]	σ [Sm^{-1}]
Bladder and Muscle	0.56	3.6	75.0	0.39
Bone	0.16	0.177	60.0	0.02

Figure 14 shows the final result for the combined method of Section 4.3 obtained after 107 iterations and 19h 30min 5s, with $\mathcal{J}(\theta) = 1.2785$. Note that the method is able to selectively heat the tumor close to the target temperature of 42.0°C, while keeping the temperature within the healthy tissues around 37.5°C. The oscillations observed in the temperature distribution and the high computational cost may be explained by the heterogeneity of the medium. The values for current densities $J_e(x_i) = \alpha_i/(\omega\mu_0)$ are in the range $[-0.0876, 0.0531]$Am^{-2}.

5.5. **Example 5: Three Breast Tumors.** In this section we test the capability of the combined method in selectively heat three breast tumors of different sizes all together. The obtained result is used later in a full transient analysis. Let us consider the breast as described in Section 5.1 with three tumors of radii 2.0cm, 1.5cm, 1.0cm and centers at $(0.28, 0.28)$, $(0.22, 0.2)$ and $(0.2, 0.28)$, respectively. See sketch in Figure 15. The material properties are the same used in previous examples, which follow summarized through Tables 1 and 4. The working frequency and number of antennas are fixed as

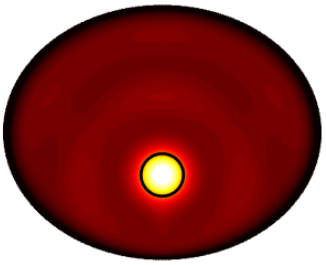

FIGURE 14. Example 4. Temperature distribution for $\omega = 300$MHz and $N = 168$. The target follows highlighted in solid black line. Obtained results for combined method. See also Figure 2(c).

$\omega = 300$MHz and $N = 168$, respectively. The thermal capacity K, specific heat of the blood c_b, perfusion rate of the blood w, electrical conductivity σ and wave number k are corrupted with 40% of White Gaussian Noise (WGN).

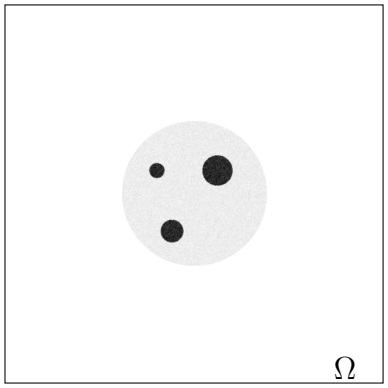

FIGURE 15. Example 5. Sketch of the healthy body and breast tumors corrupted with 40% of WGN.

5.5.1. *Steady-State Analysis.* The final current densities and the resulting temperature distribution are presented in Figure 16 for the combined method, obtained after 143 iterations and 5h 55min 50s, with $\mathcal{J}(\theta) = 1.1028$. The centers of the circles represent the positions of the antennas and their radii are proportional to the obtained current densities $\alpha^\star$. Positive sign means that the current flows out the page, otherwise the current flows into the page. From an analysis of Figure 16, it is possible to infer that the method is able to selectively heat the three tumors simultaneously even in the presence of noise, which represents an important improvement with respect to previous work by [1], where distributed antennas have been considered. The values for current densities $J_e(x_i) = \alpha_i/(\omega\mu_0)$ are in the range $[-25.8851, 36.3134]\text{Am}^{-2}$. However, less than ten antennas have relevant current densities values. See Figure 16. Therefore, it is expected that the same temperature pattern could be reached by using a smaller number of antennas.

5.5.2. *Transient Analysis.* Let us consider the obtained current density $\alpha^\star$ from the last experiment in a full transient analysis. We start by introducing the heat equation for

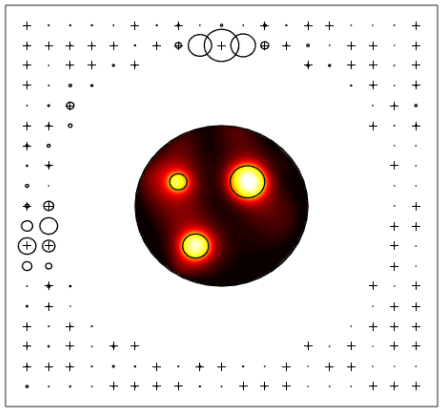

FIGURE 16. Example 5. Temperature distribution for $\omega = 300$MHz, $N = 168$ and 40% of WGN. The target follows highlighted in solid black line. The centers of the circles represent the positions of the antennas and their radii are proportional to the obtained current densities $\alpha^\star$. Finally, positive sign means that the current flows out the page, otherwise the current flows into the page. Obtained results for combined method. See also Figure 2(c).

living tissues in which the temperature $\theta : \Omega \times (0, T) \mapsto \mathbb{R}$ is solution of [25, 30]:

$$\theta \in \mathcal{V} : \int_\Omega \rho c \frac{\partial \theta}{\partial t} \eta dx + \int_\Omega \left[K \nabla \theta \cdot \nabla \eta + c_b w (\theta - \theta_b) \eta \right] dx = \frac{1}{2} \int_\Omega \sigma |u|^2 \eta dx, \quad \forall \eta \in \mathcal{V}_0 \tag{5.1}$$

where T is the final time analysis, ρ is the tissue density [kgm^{-3}] and c is the specific heat of the tissue [Jkg^{-1}°C^{-1}]. The values of ρ and c are summarized in Table 8 [7, 30]. The same values of the previous experiment are used for the others material properties, according to Tables 1 and 4. Standard backward Euler method is used in the time discretization [2]. We set $\Delta t = 1.0$s as time step for a $T = 60$ minutes of simulation and $\theta_0(x) = \theta_b$ as the initial temperature.

TABLE 8. Example 5. Physical properties for transient analysis at 300MHz of working frequency.

	ρ [kgm^{-3}]	c [Jkg^{-1}°C^{-1}]
Water	1000.0	4178.0
Tumor	1020.0	3639.0
Fat	1020.0	2387.0

The time evolution process is summarized in Figure 17. The transient period takes about 20 minutes. After that, the objective functional value converges to $\mathcal{J}(\theta) = 1.2098$, which is 10.0% higher than the one obtained in the steady-state regime. However, the temperature within the tumors are close to the target temperature. Note that at $t = 5$min, the temperature over the tumors is close to 40°C and after $t = 10$min the target temperature is reached.

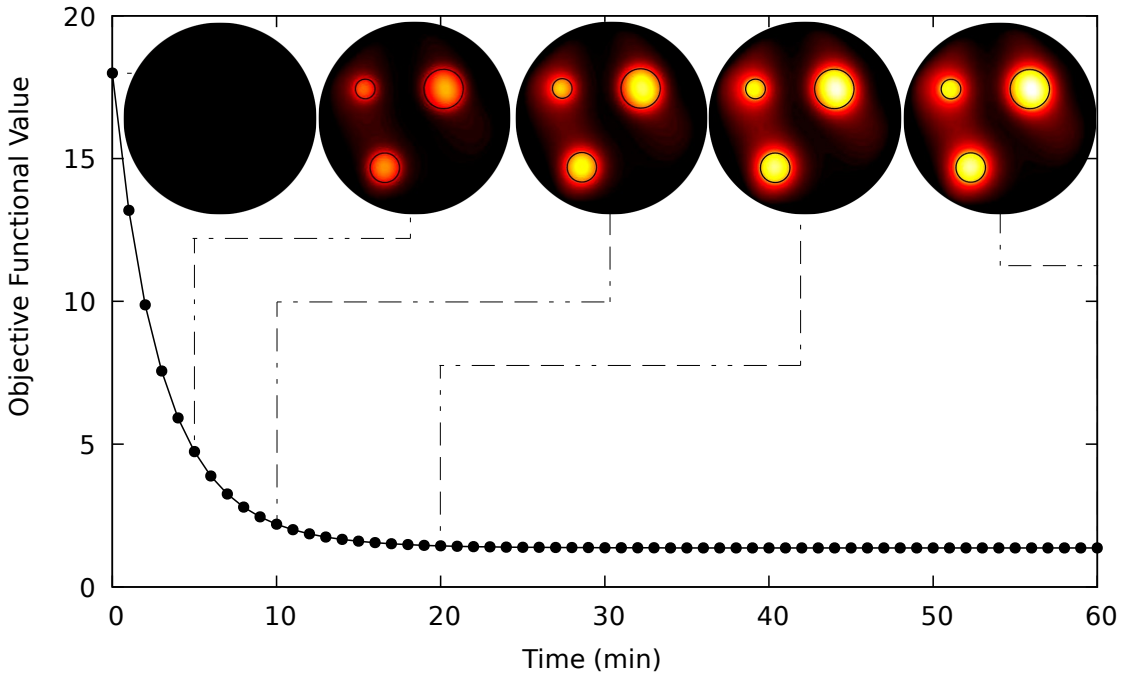

FIGURE 17. Example 5. Obtained result for the transient simulation. The temperature scale is the same as in Figure 2(c).

6. Concluding Remarks

In this paper a novel approach for pointwise antenna design in hyperthermia therapy has been proposed. The forward problem is modeled by the steady-state heat equation coupled with the Helmholtz equation. The basic idea consists in minimize a cost functional measuring the misfit between the target temperature and the temperature obtained from the model problem, with respect to the current densities passing through the antennas. The adjoint sensitivity analysis is used in order to simplify the form of the associated derivatives. In particular, the resulting sensitivities are used to devise first and second order antenna design algorithms as well as a third one that combines both the previous algorithms. Numerical experiments are presented showing different features of the proposed methodology, including its capability in selectively heating simultaneously several targets up to the desired temperature, by keeping the temperature under control in the remainder part of the body. Finally, a selected result is used in a full transient analysis, where the hot spots are keeping over the diseased tissues during the whole heating process. However, we are aware that hyperthermia therapy is a purely three dimensional phenomenon where the electromagnetic effects are governed by the Maxwell system and the material properties of living tissues may depend on the temperature, leading to more complicated non-linear forward problems. Therefore, the extension to such real-life scenarios requires further investigation, including the use of efficient numerical methods for solving the associated BVPs, as can be found in [19, Chapters 5 and 6], for instance. In addition, hyperthermia treatment also requires temperature measurements during the heating process by using inverse problem techniques [15]. Therefore, this paper can be seen as a preliminary study showing that the proposed methodology works properly in such a simplified setting.

Acknowledgments

This research was partly supported by CNPq (Brazilian Research Council), CAPES (Brazilian Higher Education Staff Training Agency) and FAPERJ (Research Foundation of the State of Rio de Janeiro). The support is gratefully acknowledged. We also thanks to Dr. Alan Amad for his contribution to this paper.

References

[1] A. A. S. Amad, A. F. D. Loula, and A. A. Novotny. A new method for topology design of electromagnetic antennas in hyperthermia therapy. *Applied Mathematical Modelling*, 42:209–222, 2017.

[2] Richard L. Burden and J. Douglas Faires. *Numerical Analysis*. The Prindle, Weber and Schmidt Series in Mathematics. PWS-Kent Publishing Company, Boston, fourth edition, 1989.

[3] C. Clason and K. Kunisch. A duality-based approach to elliptic control problems in non-reflexive banach spaces. *ESAIM: Control, Optimisation and Calculus of Variations*, 17(1):243–266, 2009.

[4] G. Danaei, S. Vander Hoorn, A. D. Lopez, C.J.L. Murray, M. Ezzati, Comparative Risk Assessment collaborating group (Cancers, et al. Causes of cancer in the world: comparative risk assessment of nine behavioural and environmental risk factors. *The Lancet*, 366(9499):1784–1793, 2005.

[5] M.S. Ferreira and J. I. Yanagihara. A transient three-dimensional heat transfer model of the human body. *International Communications in Heat and Mass Transfer*, 36(7):718–724, 2009.

[6] S. Gabriel, R.W. Lau, and C. Gabriel. The dielectric properties of biological tissues: Iii. parametric models for the dielectric spectrum of tissues. *Physics in Medicine & Biology*, 41(11):2271, 1996.

[7] Y. Gong, H. Wang, and G. Wang. Microwave heating by using flat lhm lens. In *2008 International Workshop on Metamaterials*, pages 370–373. IEEE, 2008.

[8] G. Hegyi, G.P. Szigeti, and A. Szász. Hyperthermia versus oncothermia: cellular effects in complementary cancer therapy. *Evidence-Based Complementary and Alternative Medicine*, 2013, 2013.

[9] F. Ihlenburg and I. Babuška. Finite element solution of the Helmholtz equation with high wave number part i: The h-version of the FEM. *Computers & Mathematics with Applications*, 30(9):9–37, 1995.

[10] N.A. Jaffar, N. Buniyamin, and K. Lias. An overview of available metamaterial-based antenna for non-invasive hyperthermia cancer treatment. *Indonesian Journal of Electrical Engineering and Computer Science*, 14(2):697–705, 2019.

[11] W.T. Joines, Y. Zhang, C. Li, and R.L. Jirtle. The measured electrical properties of normal and malignant human tissues from 50 to 900 MHz. *Medical physics*, 21(4):547–550, 1994.

[12] E. Jones, D. Thrall, M.W. Dewhirst, and Z. Vujaskovic. Prospective thermal dosimetry: the key to hyperthermia's future. *International Journal of Hyperthermia*, 22(3):247–253, 2006.

[13] A. Kirsch and F. Hettlich. *The Mathematical Theory of Maxwell's Equations*. Karlsruhe Institute of Technology (KIT) Karlsruhe, Germany, 2014.

[14] H. Kroeze, J.B. Van de Kamer, A.A.C. De Leeuw, and J.J.W. Lagendijk. Regional hyperthermia applicator design using fdtd modelling. *Physics in Medicine & Biology*, 46(7):1919, 2001.

[15] B. Lamien, H. Rangel Barreto Orlande, L. Antonio Bermeo Varón, R. Leite Queiroga Basto, G. Enrique Eliçabe, D. Silva dos Santos, and R. Machado Cotta. Estimation of the temperature field in laser-induced hyperthermia experiments with a phantom. *International Journal of Hyperthermia*, 35(1):279–290, 2018.

[16] T. J. Machado, J. S. Angelo, and A. A. Novotny. A new one-shot pointwise source reconstruction method. *Mathematical Methods in the Applied Sciences*, 40(15):1367–1381, 2017.

[17] MATLAB. *version 9.7.0.1216025 (R2019b) Update 1*. The MathWorks Inc., Natick, Massachusetts, 2019.

[18] N.A. Mayr, W.T.C. Yuh, T. Taoka, J.Z. Wang, D.H. Wu, J.F. Montebello, S.L. Meeks, A.C. Paulino, V.A. Magnotta, M. Adli, et al. Serial therapy-induced changes in tumor shape in cervical cancer and their impact on assessing tumor volume and treatment response. *American Journal of Roentgenology*, 187(1):65–72, 2006.

[19] P. Monk. *Finite Element Methods for Maxwell's Equations*. Numerical Mathematics and Scientific Computation. Oxford University Press, Oxford, UK, 2003.

[20] H.R. Moyer and K.A. Delman. The role of hyperthermia in optimizing tumor response to regional therapy. *International Journal of Hyperthermia*, 24(3):251–261, 2008.

[21] A. A. Novotny and J. Sokołowski. *Topological derivatives in shape optimization*. Interaction of Mechanics and Mathematics. Springer-Verlag, Berlin, Heidelberg, 2013.
[22] A. A. Novotny, J. Sokołowski, and A. Żochowski. *Applications of the topological derivative method*. Studies in Systems, Decision and Control. Springer Nature Switzerland, 2019.
[23] K. Palucka and J. Banchereau. Dendritic-cell-based therapeutic cancer vaccines. *Immunity*, 39(1):38–48, 2013.
[24] D. M. Pardoll. Cancer vaccines. *Nature medicine*, 4(5):525, 1998.
[25] H.H. Pennes. Analysis of tissue and arterial blood temperatures in the resting human forearm. *Journal of Applied Physiology*, 1(2):93–123, 8 1948.
[26] S.A. Rosenberg, J.C. Yang, and N.P. Restifo. Cancer immunotherapy: moving beyond current vaccines. *Nature medicine*, 10(9):909, 2004.
[27] J. Sokołowski and A. Żochowski. Topological derivatives for elliptic problems. *Inverse Problems*, 15(1):123–134, 1999.
[28] D.T. Tompkinsn, R. Vanderby, S.A. Klein, W.A. Beckman, R.A. Steeves, D.M. Frye B.R., and Paliwal. Temperature-dependent versus constant-rate blood perfusion modelling in ferromagnetic thermoseed hyperthermia: results with a model of the human prostate. *International Journal of Hyperthermia*, 10(4):517–536, 1994.
[29] World Health Organization. Latest global cancer data: Cancer burden rises to 18.1 million new cases and 9.6 million cancer deaths in 2018. Technical Report 263, International Agency for Research on Cancer, 2018.
[30] L. Wu, R.J. McGough, O. A. Arabe, and T. V. Samulski. An RF phased array applicator designed for hyperthermia breast cancer treatments. *Physics in Medicine and Biology*, 51(1):1–20, dec 2005.
[31] P. Wust, B. Hildebrandt, G. Sreenivasa, B. Rau, J. Gellermann, H. Riess, R. Felix, and P.M. Schlag. Hyperthermia in combined treatment of cancer. *The lancet oncology*, 3(8):487–497, 2002.

(R. Mattoso and A.A. Novotny) Laboratório Nacional de Computação Científica LNCC/MCT, Coordenação de Métodos Matemáticos e Computacionais, Av. Getúlio Vargas 333, 25651-075 Petrópolis - RJ, Brasil

Email address: {rmattoso,novotny}@lncc.br